Implications of combined solar-neutrino observations and their theoretical uncertainties

S. A. Bludman, N. Hata, D. C. Kennedy,* and P. G. Langacker
Department of Physics, University of Pennsylvania, Philadelphia, Pennsylvania 19104
(Received 6 July 1992; revised manuscript received 4 December 1992)

Constraints on the core temperature (T_c) of the Sun and on neutrino-oscillation parameters are obtained from the existing solar neutrino data, including the recent GALLEX, SAGE, and Kamiokande III results. (1) A purely astrophysical solution to the solar-neutrino problem is strongly disfavored by the data: the Homestake and Kamiokande data together are incompatible with any temperature in the Sun; the central values of both the SAGE and GALLEX results require a large reduction of T_c when they are fit to a cooler Sun. (2) Assuming the standard solar model (SSM) and matter-enhanced neutrino oscillations, the Mikheyev-Smirnov-Wolfenstein (MSW) parameters are constrained to two small regions: nonadiabatic oscillations with $\Delta m^2=(0.3\text{–}1.2)\times10^{-5}$ eV^2, $\sin^2 2\theta=(0.4\text{–}1.5)\times10^{-2}$, or large mixing-angle oscillations with $\Delta m^2=(0.3\text{–}3)\times10^{-5}$ eV^2, $\sin^2 2\theta=0.6\text{–}0.9$. The nonadiabatic solution gives a considerably better fit. For ν_e oscillations into sterile neutrinos, the allowed region (90% C.L.) is constrained to nonadiabatic oscillations. As long as the SSM is assumed, the neutrino mixing angles are at least four times larger, or considerably smaller, than the corresponding quark mixing angles. (3) Allowing both MSW oscillations and a nonstandard core temperature, (a) the experiments determine the core temperature at the 5% level, $T_c=1.02^{+0.03}_{-0.05}$ (90% C.L.) relative to the SSM, and (b) when T_c is used as a *free* parameter, the allowed MSW region is broadened: a 2% cooler Sun allows Δm^2, $\sin^2 2\theta$ implied by the supersymmetric SO(10) grand unified theory (GUT), while a 3–4% warmer Sun extends the allowed parameter space into values suggested by intermediate-scale SO(10) GUT's, for which the ν_τ may be cosmologically relevant. Superstring-inspired models are consistent with all solutions. (4) From the narrowed parameter space, we predict the neutrino spectral shape which should be observed in the Sudbury Neutrino Observatory (SNO). Expected rates for SNO, SuperKamiokande, and BOREXINO are also discussed. Throughout the calculation we use the Bahcall-Pinsonneault SSM (1992) with helium diffusion, and include nuclear and astrophysical uncertainties in a simplified, but physically transparent way.

PACS number(s): 96.60.Kx, 14.60.Gh

I. INTRODUCTION: EXPERIMENTAL STATUS AND SSM IMPROVEMENTS

Since solar neutrinos were first detected two decades ago, the observed neutrino flux has always been a factor of 1.5 to 4 times less than that predicted by the standard solar model (SSM). When both experimental and SSM uncertainties are included, the Homestake chlorine (Cl) experiment, Kamiokande, and the combined gallium result of SAGE and GALLEX respectively are approximately 6σ, 3σ, and 3.7σ below the SSM predictions. Although the GALLEX deficit is only 35%, significant differences from the SSM predictions persist. In this paper, we consider both astrophysical solutions (a cooler Sun model) and particle-physics solutions [the Mikheyev-Smirnov-Wolfenstein (MSW) effect] to the solar neutrino problem. We show that no reasonable change in the SSM can reconcile the quoted Homestake, Kamiokande, and the gallium results. On the other hand, the MSW effect, which assumes neutrino mass differences Δm^2 and mixing $\sin^2 2\theta$, accommodates all data: it does not require discarding any of the experiments, nor stretching the SSM beyond its uncertainties. Once MSW is admitted, the data determine T_c at the 5% level, yielding a value consistent with the SSM. We also discuss possible MSW parameters when a nonstandard core temperature is assumed.

There are four measurements of the solar neutrinos so far. The chlorine experiment at Homestake [1] is mainly sensitive to ^{8}B and ^{7}Be neutrinos, and reports[1] an observed rate 2.1 ± 0.3 solar neutrino units (SNU) (0.26 ± 0.04 of the SSM), while the SSM prediction is 8.0 ± 1.0 SNU [2]. (Quoted errors are all 1σ in this paper.) A direct counting measurement by the Kamiokande Collaboration observes Čerenkov light from recoil electrons scattered by ^{8}B neutrinos. The combined result of Kamiokande II [3] and 395 days of Kamiokande III [4] is 0.50 ± 0.07 of the central value of the SSM; there is an additional 14% uncertainty in the SSM prediction. A unique opportunity to observe low-energy *pp* neutrinos, which come from the main reaction responsible for the energy generation in the Sun, is provided by the SAGE and GALLEX gallium experiments. The GAL-

*Present address: Fermi National Accelerator Laboratory, P.O. Box 500 MS106, Batavia, IL 60510.

[1]We ignore the possibility of time dependence in the Homestake data.

LEX result is 83±21 SNU (0.63±0.16 of the SSM) [5], again well below the SSM value 132^{+7}_{-6} SNU. SAGE has published a lower value 20^{+35}_{-38} SNU based on their first five extractions [6]. The most recent SAGE result from 1991 data is 85^{+30}_{-38} SNU [7], which is one standard deviation higher than the previous result and consistent with the GALLEX result. The cumulative result of SAGE is 58^{+22}_{-28} SNU. When all SAGE and GALLEX data are combined, the gallium result is 71±15 SNU.

The SSM itself has undergone several refinements over the years. There are presently at least four SSM's [2,8–10], which, for the same physics input, agree with each other within 1% [2] and agree with the speed of sound calculated in p-mode helioseismology within 2% [11]. The latest published solar model by Bahcall and Pinsonneault improves on earlier calculations by using the most recent OPAL calculated opacities, meteoritic iron abundances, and updated nuclear-reaction cross sections [2]. The new model includes the effects of helium diffusion so that the observed ^{3}He surface abundance is obtained. Their prediction for the convective zone boundary is in striking agreement with helioseismology data [12]. The surface abundances of the ^{7}Li and ^{9}Be are still overestimated, but the surface abundances have negligible effect on the neutrino production in the core.

II. COOLER SUN WILL NOT EXPLAIN THE OBSERVED NEUTRINO FLUXES

The production of high energy ^{8}B neutrinos is directly proportional to the ^{3}He $(\alpha,\gamma)^7$Be and ^{7}Be$(p,\gamma)^8$B nuclear cross sections and the production of intermediate energy ^{7}Be neutrinos is proportional to the ^{3}He$(\alpha,\gamma)^7$Be cross section. Those productions depend sensitively on the solar temperature in the innermost 5% of the Sun's radius. This inner core temperature is not probed by existing p-wave helioseismological observations, but is determined by the radiative opacities throughout the Sun, which are believed to be calculated to within a few percent [2].

Many nuclear and astrophysical explanations have been proposed to explain the solar neutrino deficit. One possibility is to change input parameters, such as lowering the ^{7}Be$(p,\gamma)^8$B cross section or reducing the opacity. Another is to invoke mechanisms that are not included in the SSM, such as a large core-magnetic field, a rapidly rotating core, or hypothetical weakly interacting massive particles (WIMP's) which carry away energy from the core. The net effect is usually a lowering of the core temperature and thus a reduction of the nuclear burning taking place there.

It is therefore reasonable to examine the core temperature as a diagnostic of a whole class of astrophysical explanations of the neutrino deficit, although the temperature profile is the result, not an input, of a solar model [13]. We choose the central temperature (T_c) as a phenomenological parameter representing different conceivable solar models. We simplify the model by ignoring changes in the temperature profile and in the distribution of chemical compositions in the core, although the effects may be non-negligible in some cases such as WIMP scenarios [14]. The approximate correlation of the neutrino fluxes with T_c was obtained by Bahcall and Ulrich [8] by examining 1000 self-consistent SSM's with randomly distributed input parameters, and is given as simple power laws [8]:

$$\phi(pp)\sim T_c^{-1.2},\quad \phi(^7\mathrm{Be})\sim T_c^{8},\quad \phi(^8\mathrm{B})\sim T_c^{18}\ . \tag{1}$$

For each experiment we therefore parametrize rates relative to the SSM as functions of T_c:

$$R_{\mathrm{Cl}}=(1\pm0.033)[0.775\times(1\pm0.100)\times T_c^{18}+0.150\times(1\pm0.036)\times T_c^{8}+\text{small terms}]\ ,$$

$$R_{\mathrm{Kam}}=(1\pm0.100)\times T_c^{18}\ ,$$

$$R_{\mathrm{Ga}}=(1\pm0.04)[0.538\times(1\pm0.002)\times T_c^{-1.2}+0.271\times(1\pm0.036)\times T_c^{8}$$
$$+0.105\times(1\pm0.100)\times T_c^{18}+\text{small terms}]\ ,$$

where T_c is the central temperature relative to the SSM ($T_c=1\equiv15.67\times10^6$ K). The Bahcall-Pinsonneault solar model including diffusion [2] is used throughout the paper, unless otherwise mentioned. The uncertainty in the overall factors for Cl and Ga is due to the detector reaction cross sections. The uncertainties in each neutrino flux include only nuclear physics uncertainties in production cross sections; astrophysical uncertainties are absorbed into a variable T_c. These flux uncertainties are properly correlated for the three experiments. The "small terms" represent the neutrinos from pep and CNO reactions, which contribute to the Cl rate ~2.5% and ~5%, respectively, and to the Ga rate ~2.4% and ~6%, respectively. The T_c dependence of these fluxes are not given in Ref. [8]. We take the pep flux constant in T_c and have examined two extreme cases for the CNO fluxes: $\phi(\mathrm{CNO})\sim$const and $\phi(\mathrm{CNO})\sim T_c^{18}$. Both cases yield essentially the same conclusions, and in the rest of the paper we take $\phi(\mathrm{CNO})\sim$const.

The T_c dependence of the Kamiokande, Cl, and Ga detectors are each shown in Fig. 1, and the best fits for various combinations of the data are summarized in Table I. If each experiment were fit alone, Kamiokande and Homestake require a reduction of T_c by 4±1% and 10±1%, respectively. For the gallium experiments SAGE and GALLEX, T_c must be reduced by 14±10% and 13±11%, respectively, but still do not completely fit the data, because the negative exponent of T_c in the pp flux works against the reduction of the total rate. When T_c is reduced, in order to match the observed luminosity, the pp chain has to compensate the energy loss due to reductions of the other reactions. As a result the T_c

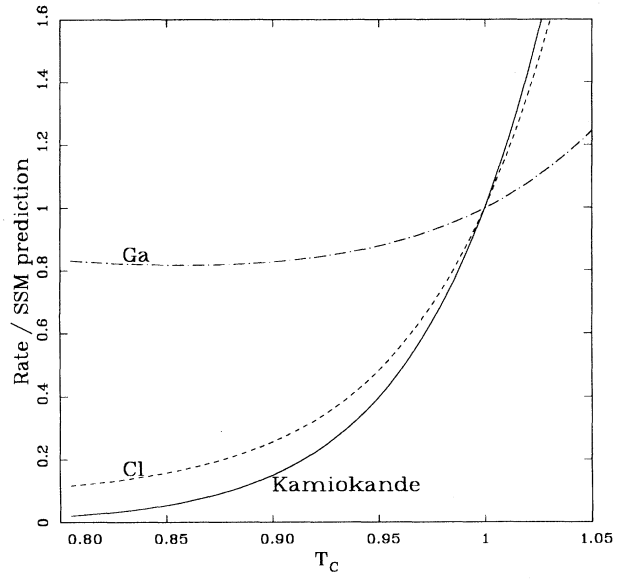

FIG. 1. The approximate T_c dependence of the neutrino counting rates (relative to the SSM) for the Cl, Ga, and Kamiokande experiments, according to the power laws [Eq. (1)]. T_c is relative to the SSM value ($T_c=1=15.67\times10^6$ K$=1.35$ keV).

reduction fails to fit the central value of the gallium rate, although it is compatible with the upper end of the range. The three separate T_c fits for Kamiokande, Homestake, and the combined gallium results are, respectively, 3σ, 6σ, and 1.7σ below the SSM prediction $T_c=1\pm\Delta T_c$, where the SSM uncertainty $\Delta T_c=0.0057$ is estimated from the 1000 SSM calculations in Ref. [15].

The combined observations cannot be fit by any single T_c. The larger Kamiokande rate relative to the Cl rate especially contradicts the T_c dependence shown in Fig. 1. The simultaneous fit of Kamiokande and Cl yields $T_c=0.92\pm0.01$, but the χ^2 value is so large ($\chi^2=13.78$) as to exclude the fit at the $>99.99\%$ C.L. The combined Kamiokande and GALLEX results yield a marginally consistent T_c: the best fit is $T_c=0.96\pm0.01$ with $\chi^2=2.64$ (89.3% C.L.). When all three experiments are fit simultaneously, $T_c=0.92\pm0.01$ but the χ^2 test rejects the cooler Sun hypothesis at 99.99% C.L. This strong rejection of the cooler Sun is driven mainly by the contradiction between Kamiokande and Homestake.

In our fit, T_c is allowed to vary in a range much wider than that for which the power laws [Eq. (1)] were derived by Bahcall and Ulrich. For such large changes in T_c, the power laws do not guarantee the consistency of the solar models with the observed luminosity. In fact the consistency is better maintained by keeping the sum of the neutrino fluxes constant, rather than using the power law for the *pp* flux. Table II shows the T_c fits when the sum of the major fluxes (*pp* and ^{7}Be) are kept constant while the ^{7}Be flux is changed according to the power law. The best fit value of the GALLEX data is now 0.66, but with a large uncertainty (0.64). The GALLEX result is compatible with the cooler Sun model because of the large experimental error, but, in order to fit its central value, T_c has to be reduced this much to eliminate all neutrinos from ^{7}Be and ^{8}B.

We also stress that our conclusions do not depend on a specific choice of the flux exponents [Eq. (1)]. We have investigated the cooler Sun model with various combinations of the exponents. Provided only that the ^{7}Be flux is less temperature dependent than the ^{8}B flux, the Cl rate is expected to be larger than the Kamiokande rate, contradicting the data [16]. Even if both flux components had the same temperature exponent ($=18$) while keeping the sum of *pp* and ^{7}Be fluxes constant, we find that $T_c=0.93\pm0.01$ and $\chi^2=10.2$ for one degree of freedom: the χ^2 test excludes the fit at 99.9% C.L. For the combined results of all four experiments, $T_c=0.93\pm0.01$ and $\chi^2=12.3$ (99.8% for two degrees of freedom). Our conclusion remains the same for other combinations of the exponents. We have examined two other choices of the exponents: for $\phi(\mathrm{Be})\sim T_c^{10}$ and $\phi(\mathrm{B})\sim T_c^{20}$, the best-fit value for the combined results is $T_c=0.93\pm0.01$ with $\chi^2=16.4$ ($>99.99\%$); for $\phi(\mathrm{Be})\sim T_c^{15}$ and $\phi(\mathrm{B})\sim T_c^{27}$, $T_c=0.95\pm0.01$ and $\chi^2=15.8$ ($>99.99\%$).

To see the effect of the nuclear cross-section uncertainties on the T_c fit, we have repeated the fits doubling the nuclear cross-section errors, and found that the results

TABLE I. The T_c fits for various combinations of the Homestake (Cl), Kamiokande II+III (Kam), SAGE, and GALLEX results. Listed are the best fit value of T_c with 1σ error, χ^2 values, and confidence levels of excluding the fits.

	$T_c\pm\Delta T_c$	χ^2	C.L. (%)
Kam	0.96±0.01	0	· · ·
Cl	0.90±0.01	0	· · ·
SAGE	0.86±0.10	3.2	· · ·
GALLEX	0.87±0.11	1.3	· · ·
SAGE+GALLEX	0.86±0.08	3.7	95
Kam+Cl	0.92±0.01	13.8	>99.9
Kam+GALLEX	0.96±0.01	2.6	89
Cl+GALLEX	0.90±0.01	1.5	77
Kam+Cl+GALLEX	0.92±0.01	15.5	>99.9
Kam+Cl+SAGE+GALLEX	0.92±0.01	18.2	>99.9

TABLE II. The T_c fits when the sum of the major neutrino fluxes (pp and ^{7}Be) is kept constant. The ^{7}Be and ^{8}B fluxes are changed according to the power law.

	$T_c \pm \Delta T_c$	χ^2	C.L. (%)
Kam	0.96±0.01	0	· · ·
Cl	0.90±0.01	0	· · ·
SAGE	0.57±0.61	1.2	· · ·
GALLEX	0.66±0.64	0.1	· · ·
SAGE+GALLEX	0.60±0.47	0.7	59
Kam+Cl	0.92±0.01	13.8	>99.9
Kam+GALLEX	0.96±0.01	2.4	88
Cl+GALLEX	0.90±0.01	0.9	65
Kam+Cl+GALLEX	0.92±0.01	15.0	>99.9
Kam+Cl+SAGE+GALLEX	0.92±0.01	17.2	>99.9

are almost identical to Table I and Table II; this is because the dominant cross-section uncertainties [^{7}Be$(p,\gamma)^8$B and ^{3}He$(\alpha,\gamma)^7$Be] are strongly correlated between the Cl rate and Kamiokande rate, and cannot resolve the discrepancy of their results. Based on these observations one can conclude that the cooler Sun model, which is a nearly universal feature of astrophysical solutions to the solar neutrino problem, is strongly disfavored by the data: the combined result of Homestake and Kamiokande is incompatible with the cooler Sun hypothesis, and to explain the central value of the gallium data, the cooler Sun hypothesis requires a gross reduction of T_c.

III. MSW FIT TO THE COMBINED OBSERVATIONS

While modifications of the solar model cannot accommodate the data, an attractive solution is proposed from particle physics. Matter-enhanced neutrino oscillation (MSW effect), first proposed by Wolfenstein, then applied to solar neutrinos by Mikheyev and Smirnov, offers a natural explanation of the observed solar neutrino deficit without requiring any *ad hoc* mechanisms [17]. This MSW mechanism assumes new properties of neutrinos, mass and mixings, to convert electron-neutrinos to other species when the neutrinos propagate through the Sun, making possible a large reduction of the ν_e-counting rate. The MSW assumption of neutrino mass and mixing is a natural extension of the standard model, and requires no *ad hoc* features such as a large magnetic moment. Unlike vacuum oscillations, it does not require fine-tuning. If the MSW oscillation takes place in the Sun, the determination of the neutrino mass and mixing will provide a clue to grand unified theories, which naturally lead to parameters in the relevant region [16,18].

The MSW effect depends on two intrinsic neutrino parameters: the mass-squared difference Δm^2 and the vacuum mixing angle θ between ν_e and another neutrino species into which it converts. In these calculations, instead of solving the Schrödinger equation for the oscillations numerically, we employ the Parke formula [19] $P(E)=\frac{1}{2}+(\frac{1}{2}-P_j)\cos 2\theta_M \cos 2\theta$ for the survival probability of ν_e with energy E, where the matter mixing angle θ_M is defined by

$$\tan 2\theta_M = \frac{\sin 2\theta}{\cos 2\theta - 2\sqrt{2} G_F n_e^0 E/\Delta m^2} ;$$

G_F is the Fermi coupling constant and n_e^0 is the electron density at the ν_e production radius. Here we use the Landau-Zener jump probability $P_j = e^{-\chi}$ [20], where the adiabaticity $\chi = \pi h \sin^2\theta \Delta m^2/E$ and $h = (-d \ln n_e/dr)^{-1}$ is the electron-density scale height evaluated at the resonance radius. (This formula agrees with the exact solution for large mixing angles and with the linear Landau-Zener approximation [21] for small mixing angles.)

The conversion occurs in a wide parameter space that covers four orders of magnitude both in Δm^2 and $\sin^2 2\theta$: a triangle-shaped region in the $\sin^2 2\theta$ versus $\Delta m^2/E$ plane, surrounded by $\Delta m^2/E \leq 2\times 10^{-5}$ (eV^2/MeV) and $\sin^2 2\theta\, \Delta m^2/E \geq 10^{-9}$ (eV^2/MeV). Typical survival-probability contours are shown in the Δm^2 versus $\sin^2 2\theta$ plane (MSW diagram) after integrations over the neutrino production site and the neutrino energy, including the detector cross sections. The spatial distribution of neutrino production and the electron density in the Sun are taken from Bahcall and Pinsonneault [2]. The detector cross sections are taken from Bahcall and Ulrich [8]. For Kamiokande, the ν_μ (or ν_τ) contribution for flavor oscillations, the energy threshold, the energy resolution, and the trigger efficiency are all properly included [22].

The MSW diagrams show three physically distinct regions: the adiabatic region (the horizontal upper arm of the triangle), the nonadiabatic region (the diagonal arm), and the large-mixing region (the right, vertical arm). For the adiabatic solution, the MSW resonance takes place in the core of the Sun where the neutrinos are produced; the density is high enough for the higher-energy neutrinos to resonate and be depleted while the lower-energy ones survive. For the nonadiabatic solution, the higher-energy neutrinos survive more because of nonadiabatic (Landau-Zener) jumping. In the large-mixing region, which connects smoothly to vacuum oscillation, the neutrino spectrum is equally reduced over the whole spectrum. In the middle of the isoprobability triangle, almost 100% conversion of ν_e occurs.

This flexibility makes the MSW effect phenomenologically robust. It can preferentially suppress the high-energy (^{8}B) neutrinos, or the low-energy (^{7}B and pp) neu-

trinos more. It can deplete the lower-energy part of the ^{8}B and ^{7}Be spectrum while keeping the *pp* flux, as suggested by the experiments (Fig. 17).

In fitting the data, theoretical uncertainties of the SSM are treated with care, using a simple and transparent parametrization. For each flux component the nuclear cross-section uncertainties of every reaction are added quadratically to the detector cross-section uncertainties and to the astrophysical (non-nuclear) uncertainties. The latter is represented by the uncertainty in the central temperature ΔT_c times the exponent defined in Eq. (1). The theoretical uncertainty $\Delta T_c = 0.0057$ is chosen to yield flux uncertainties consistent with those given in Ref. [2], and to be consistent with estimates from the 1000 SSM Monte Carlo calculations of Bahcall and Ulrich [15]. The correlations of the uncertainties among the experiments and flux components are properly taken into account. Our calculations were compared with other studies which utilize 1000 Monte Carlo SSM's [23,24]; the agreement is excellent.

Effects of the astrophysical uncertainties on the MSW effect were also examined. Both the uncertainties from the neutrino production profile, which affects the matter mixing angle at the neutrino production, and from the electron-density scale height, which enters in the jump probability, were found to be small.

Survival-probability contours and 90%-C.L. allowed regions are shown for each experiment in Figs. 2, 3(a), 4, and 5. The Homestake allowed region (Fig. 2) does not precisely trace the isoprobability, contour because of the difference in ^{7}Be and ^{8}B theoretical uncertainties. Fig. 3(a) and 3(b) show the Kamiokande result for flavor oscillations and oscillations to sterile neutrinos, respectively.

The combined result (90% C.L.) of Homestake, Kamiokande II+III, SAGE, and GALLEX is displayed in Fig. 6(a). The confidence-level region is defined from χ^2 values that satisfy $\chi^2(\sin^2 2\theta, \Delta m^2) = \chi^2_{\min} + 4.6$, which is valid in the approximation that the allowed regions are "ellipses" on the $\ln \sin^2 2\theta - \ln \Delta m^2$ plane. Including the GALLEX observations, the allowed MSW parameters are either $\Delta m^2 = (0.3-1.2)\times 10^{-5}$ eV^2, $\sin^2 2\theta = (0.4-1.5)\times 10^{-2}$ (nonadiabatic solution), or $\Delta m^2 = (0.3-3)\times 10^{-5}$ eV^2, $\sin^2 2\theta = 0.6-0.9$ (large-mixing solution). The best fits of Δm^2 and $\sin^2 2\theta$ along with the χ^2 value for each region are listed in the second and third columns of Table III. The experiments prefer the nonadiabatic solution to the large-angle solution. The nonadiabatic

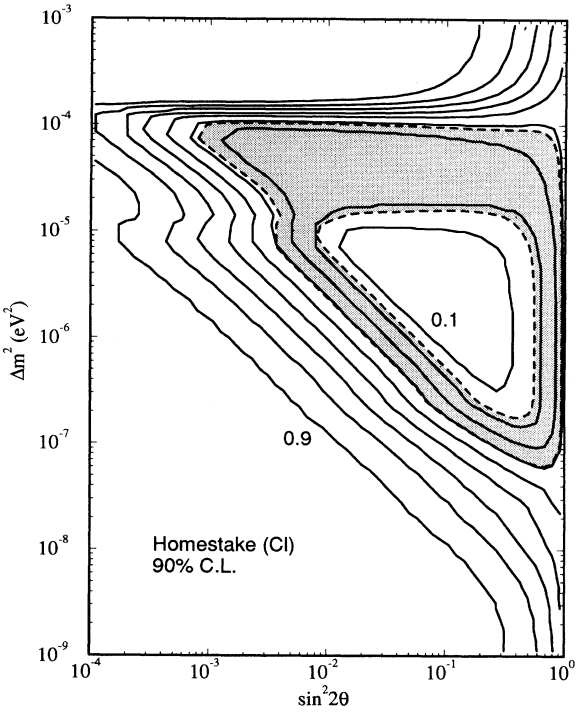

FIG. 2. The ν_e survival probability contours (solid lines) for Cl experiments and the allowed region obtained from the Homestake result (90% C.L., shaded region). The contours are for survival probabilities of 0.1, 0.2, . . . , 0.9, starting with the innermost solid line. The calculation of the allowed region includes the experimental errors, the detector cross section uncertainties, and the SSM flux errors. The allowed region slightly deviates from the isoprobability contours because of the difference in the ^{7}Be and ^{8}B flux uncertainties.

MSW solution yields a good fit ($\chi^2 = 0.69$), but in the large-mixing region, the χ^2 value is large ($\chi^2 = 3.81$); it is allowed at the 90% C.L. by the definition above, but for one degree of freedom (=three experiments minus two parameters) this region is excluded at 95% C.L. The allowed regions at the 68, 90, 95, and 99% C.L. are shown in Fig. 6(b): there is no parameter allowed in the large-angle region at 68% C.L. The combined fit without theoretical uncertainties from the SSM and detector cross sections is displayed in Fig. 6(c). Comparison with Fig. 6(a) shows the noticeable effect of SSM uncertainties.

TABLE III. The best fit of the Homestake, Kamiokande II+III, SAGE, and GALLEX results. In the T_c=SSM [$T_c = 1 \pm 0.0094$ (90% C.L.)] column, shown are the best fit of Δm^2 and $\sin^2 2\theta$ with the χ^2 value for each of the allowed MSW regions. The T_c=free column is for the three parameter fit (Δm^2, $\sin^2 2\theta$, and T_c). The T_c errors are at 90% C.L.

	T_c=SSM		T_c=free	
	Nonadiabatic	Large mixing	Nonadiabatic	Large mixing
$\sin^2 2\theta$	8.3×10^{-3}	0.76	1.1×10^{-2}	0.38
Δm^2 (eV^2)	4.9×10^{-6}	9.8×10^{-6}	5.8×10^{-6}	9.3×10^{-6}
$T_c \pm \Delta T_c$ (90% C.L.)	1 ± 0.0094	1 ± 0.0094	$1.02^{+0.03}_{-0.05}$	$1.04^{+0.03}_{-0.04}$
χ^2	0.69	3.81	0	0

TABLE IV. The best fit of the Homestake, Kamiokande II+III, SAGE, and GALLEX results for sterile-neutrino oscillations. In the T_c=SSM [$T_c=1\pm0.0094$ (90% C.L.)] column, shown are the best fit of Δm^2 and $\sin^2 2\theta$ with the χ^2 value for each of the allowed MSW regions. The T_c=free column is for the three parameter fit (Δm^2, $\sin^2 2\theta$, and T_c). The T_c errors are at 90% C.L.

	T_c=SSM		T_c=free	
	Nonadiabatic	Large mixing	Nonadiabatic	Large mixing
$\sin^2 2\theta$	9.1×10^{-3}	0.85	9.8×10^{-3}	. . .
Δm^2 (eV^2)	4.1×10^{-6}	5.5×10^{-6}	4.0×10^{-6}	. . .
$T_c\pm\Delta T_c$ (90% C.L.)	1 ± 0.0094	1 ± 0.0094	$1.00^{+0.16}_{-0.03}$	. . .
χ^2	3.64	10.27	3.66	. . .

Considering possible systematic errors correlated among the two gallium experiments, we have also fit the data using the SAGE and GALLEX data separately. Omitting SAGE gives almost identical result [Fig. 6(d)]. Our Fig. 6(a) practically agrees with that obtained by the GALLEX group [5], who included the day-night effect and ν_e regeneration in the Earth, which we have neglected.

Allowed regions for various combinations of any two experiments are shown in Fig. 7 (Kamiokande and Homestake), Fig. 8 (Kamiokande and the gallium experiments), and Fig. 9 (Homestake and the gallium experiments).

We have also examined possibilities of oscillations to a sterile neutrino [25,26]. If ν_e oscillates into a sterile neutrino instead of ν_μ or ν_τ, the term $n_e-n_n/2$ enters the MSW equation in place of n_e. (Here n_e and n_n are the local electron and neutron densities in the Sun [25].) Also, for the Kamiokande detector there is no neutral current contribution from the converted neutrinos. The result for ν_e oscillations into sterile neutrinos is displayed in Fig. 3(b) for Kamiokande, and in Fig. 10 and Table IV for the combined fit. (There is no significant change for

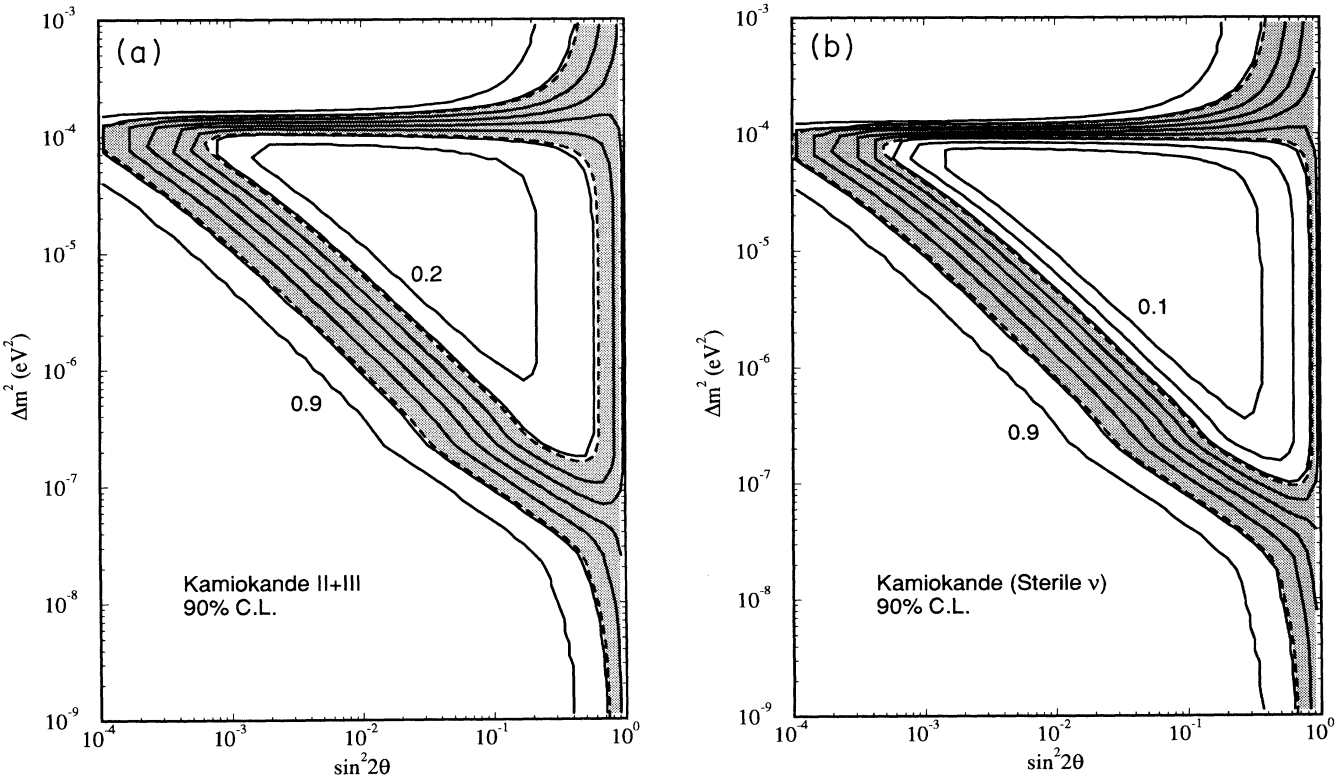

FIG. 3. (a) The ν_e survival probability contours (solid lines) for Kamiokande experiments and the allowed region for the Kamiokande II and III (395 days) result (90% C.L. shaded region). This is for flavor oscillations into ν_μ or ν_τ. The contours are for effective survival probabilities of 0.2, 0.3, . . . , 0.9, which include the effects of neutral current scattering. (There is no 0.1 contour.) The calculation includes the energy threshold, the energy resolution, and the trigger efficiency. The allowed region includes the SSM uncertainties of the ^{8}B flux. (b) Same as (a), except that it is for oscillations into a sterile neutrino. The contours are for survival probabilities of 0.1, 0.2, . . . , 0.9. Compared to flavor oscillations, lack of a neutral current contribution increases the ν_e survival probability required by the data and therefore pushes the allowed region outward of the triangle.

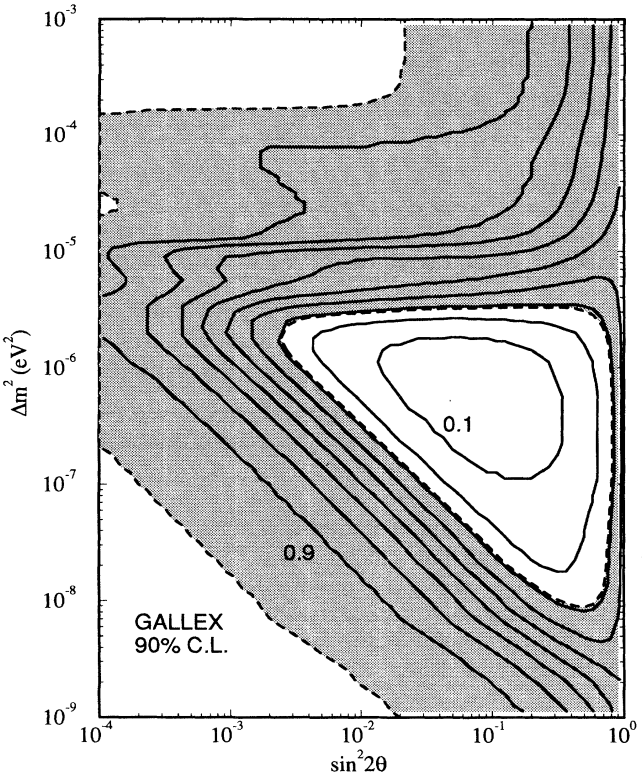

FIG. 4. The ν_e survival probability contours (solid lines) for Ga experiments and the 90% C.L. allowed region for the GALLEX result. The calculation of the allowed region includes the experimental errors, the detector cross-section uncertainties, and the SSM flux errors. The contours are for survival probabilities of 0.1, 0.2, . . . , 0.9.

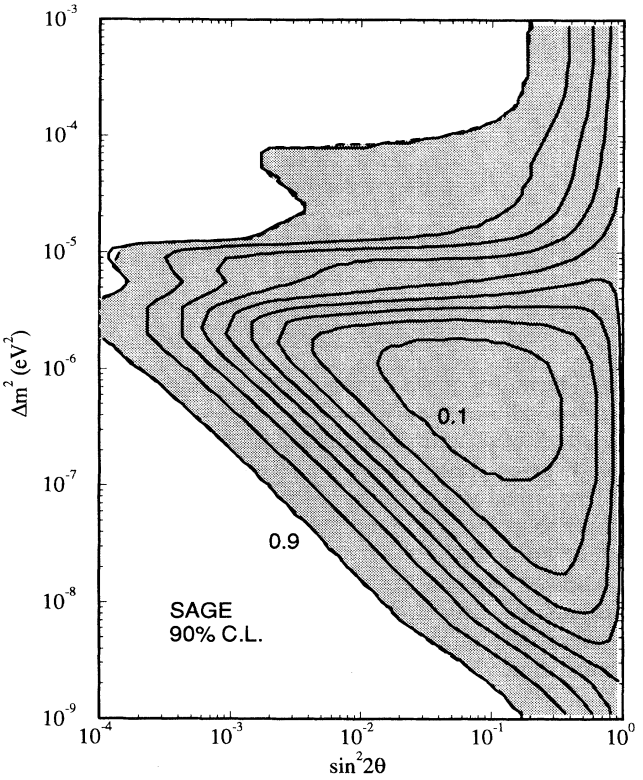

FIG. 5. Same as Fig. 4, except the allowed region is for SAGE.

the Homestake and GALLEX experiments.) Because of the constraints by the Kamiokande observations, there is no solution in the large-angle region at 90% C.L., and the allowed parameters are limited in the nonadiabatic region. Even in the nonadiabatic region, the best fit yields $\chi^2=3.64$ and is excluded at 94% C.L. for one degree of freedom. This is because of the smaller Homestake rate relative to Kamiokande: the absence of the neutral current events in Kamiokande requires a larger ν_e survival probability than for the flavor-oscillation case, and therefore widens the discrepancy between the two experiments.

The precise determination of MSW parameters will allow us to draw some theoretical conclusions in Sec. V and to make predictions for next-generation neutrino experiments in Sec. VI.

IV. SIMULTANEOUS FIT OF MSW AND CORE TEMPERATURE

We have also studied the possibilities of having both MSW oscillations *and* a nonstandard solar model by allowing T_c to be a completely free parameter. (We use the same nuclear and detector uncertainties as in the SSM case, and the sum of the *pp* and ^{7}Be fluxes are fixed, rather than using the power law for the *pp* flux.) The data are fit simultaneously to three parameters Δm^2, $\sin^2 2\theta$, and T_c. The χ^2 plot is displayed as a function of T_c (Fig. 11), where χ^2 is minimized for each T_c with respect to Δm^2 and $\sin^2 2\theta$ in the allowed region in the MSW diagram. By the χ^2 fit, the data determine the core temperature at the 5% level. The best fits are $T_c=1.02^{+0.03}_{-0.05}$ (90% C.L.) in the nonadiabatic region and $T_c=1.04^{+0.03}_{-0.04}$ in the large-mixing region, in good agreement with the SSM prediction $T_c=1\pm0.0057$ (1σ). The consistency between the data and the SSM is encouraging. Moreover, even allowing the MSW conversion and the other uncertainties, the observations determine the core temperature to within 5% [27].

The allowed region for the three-parameter fit is shown in Fig. 12. For each Δm^2 and $\sin^2 2\theta$, the χ^2 is minimized with respect to T_c, and $\chi^2(\sin^2 2\theta, \Delta m^2)=\chi^2_{\min}+4.6$ determines the 90% C.L. allowed region, where $\chi^2_{\min}$ is a minimum with respect to all three parameters. By allowing T_c to be a free parameter, the two allowed regions are widened, now stretching over $\sin^2 2\theta=(0.1-2)\times10^{-2}$ and 0.07–0.9, and $\Delta m^2=(0.2-2.5)\times10^{-5}$ eV^2. (At 96% C.L., the two regions merge into one.) The best-fit parameters are shown in Tables III and IV. The T_c dependence of the region is seen in Fig. 13(a) and Fig. 13(b), which shows the 90% C.L. contours when T_c is fixed at 1.05 and 0.95 respectively. The higher tempera-

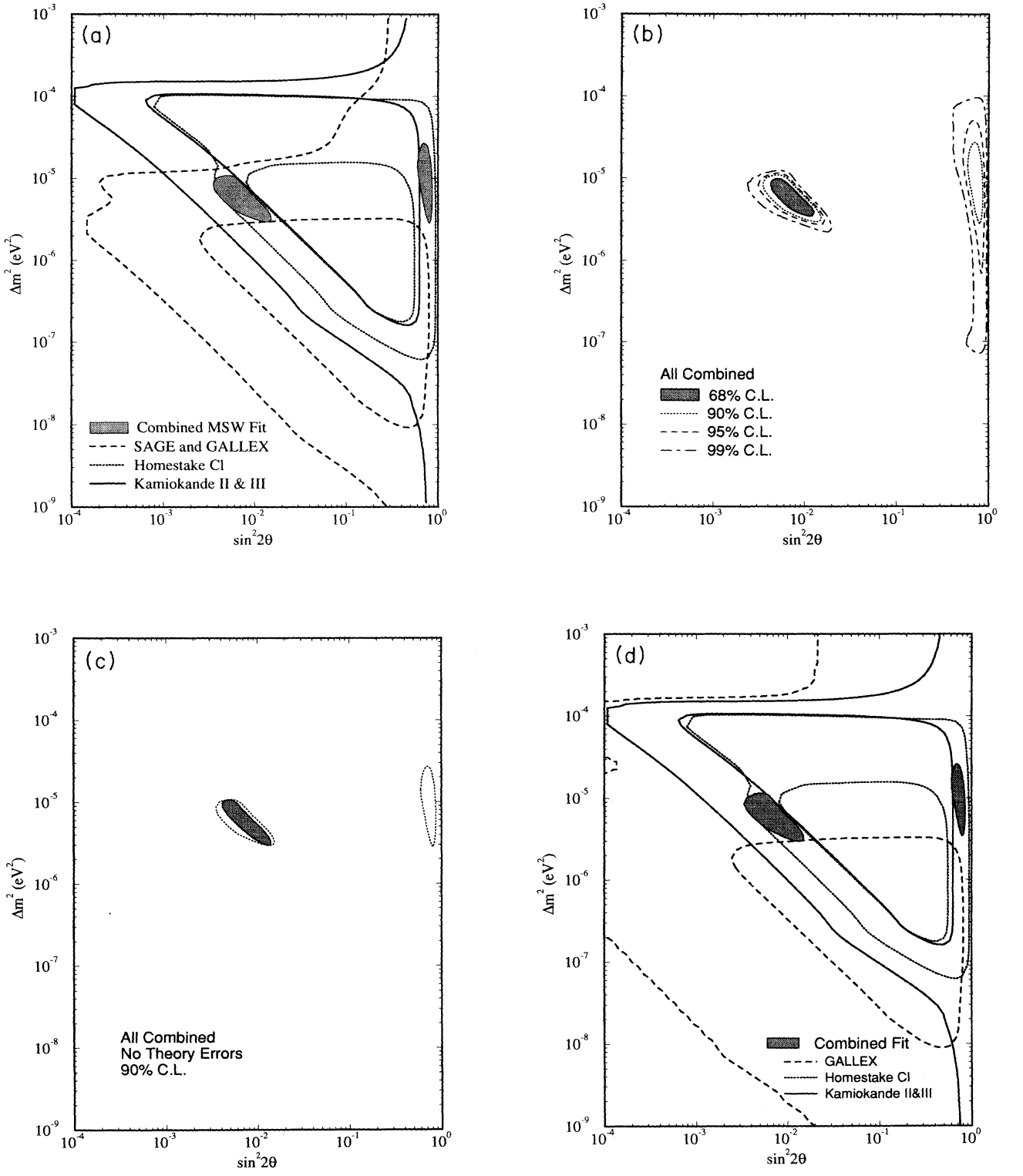

FIG. 6. (a) The allowed region for Homestake (dotted region), Kamiokande II+III (solid line), and the combined SAGE and GALLEX (dashed line) results. The shaded region is the combined fit of the four experiments (90% C.L.). (b) The allowed region of combined Homestake, Kamiokande II+III, SAGE, and GALLEX results at 68% (shaded region), 90% (dashed lines), 95% (dotted lines), and 99% (dash-dotted lines) C.L. (c) The allowed region of the combined results *with* (dotted line) and *without* (shaded regions) theoretical uncertainties from the SSM and the detector cross sections. Without theoretical uncertainties, there is no allowed large-angle region at 90% C. L. (d). The allowed region of the combined Homestake, Kamiokande II+III, and GALLEX (but not SAGE) results at 90% C.L.

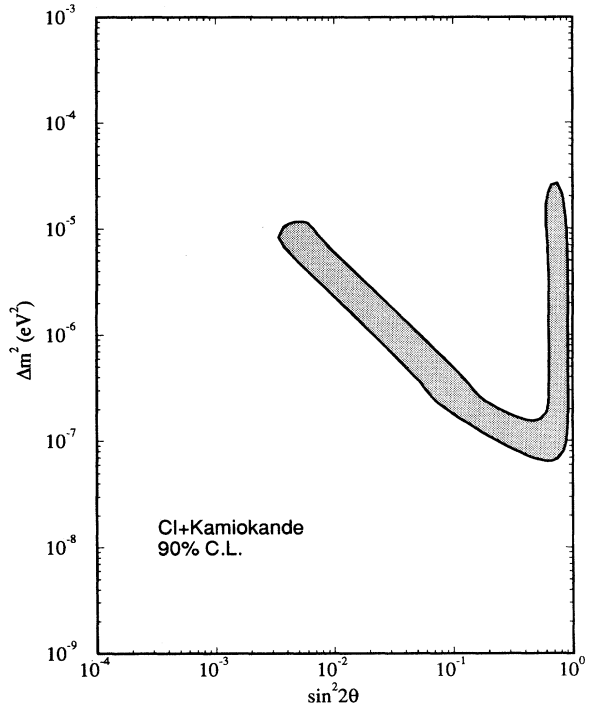

FIG. 7. The combined fit of the Kamiokande II+III and Homestake results (90% C.L.).

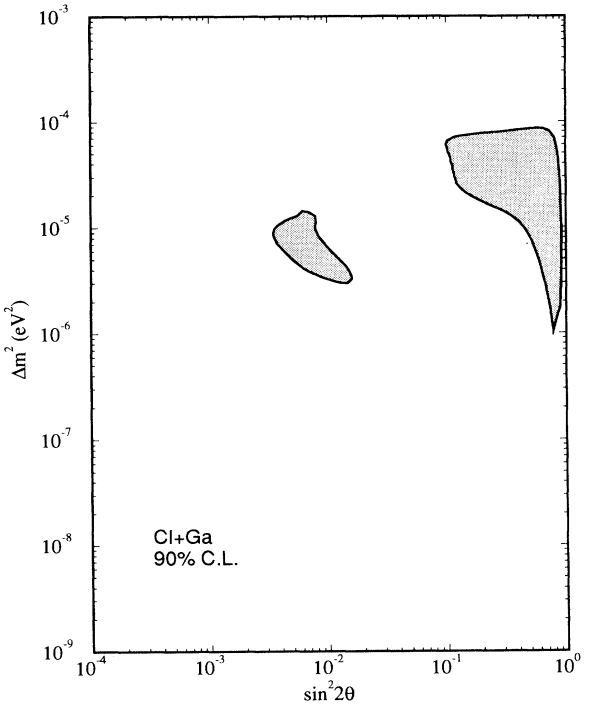

FIG. 9. The combined fit of the Homestake and the gallium (SAGE and GALLEX) results (90% C.L.).

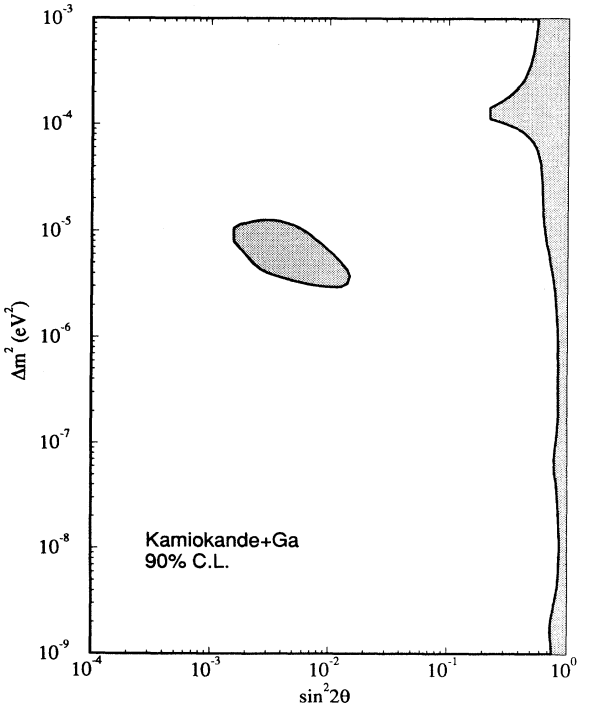

FIG. 8. The combined fit of the Kamiokande II+III and the gallium (SAGE and GALLEX) results (90% C.L.).

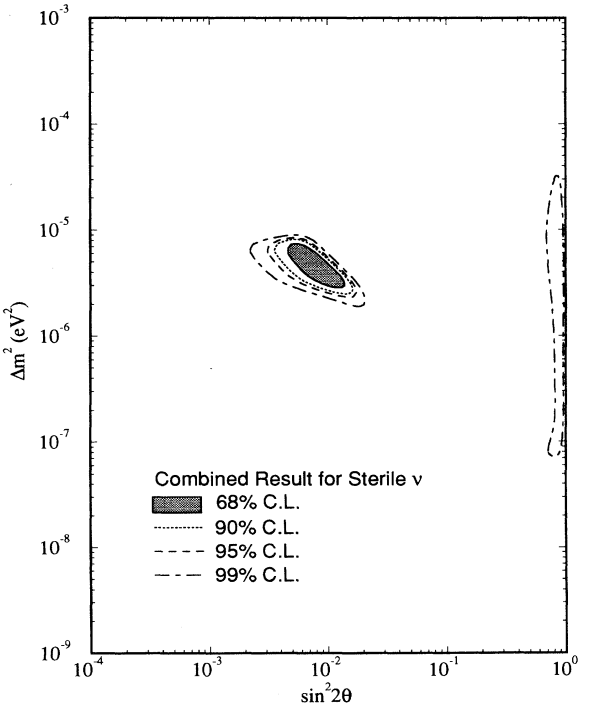

FIG. 10. The fit to oscillations to sterile neutrinos at 68% (shaded), 90% (dashed line), 95% (dotted line), and 99% (dash-dotted lines) C.L. The data are the combined result of the Homestake, Kamiokande II+III, SAGE, and GALLEX.

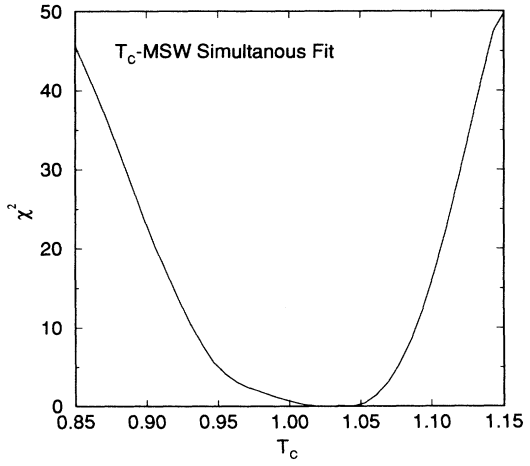

FIG. 11. The χ^2 plot as a function of T_c in the three parameter fit (T_c, Δm^2, and $\sin^2 2\theta$) of the Homestake, Kamiokande, SAGE, and GALLEX. For each T_c, the χ^2 is minimized with respect to Δm^2 and $\sin^2 2\theta$. The data determine T_c within $0.97 \leq T_c \leq 1.05$ (90% C.L.), which is consistent with the SSM value.

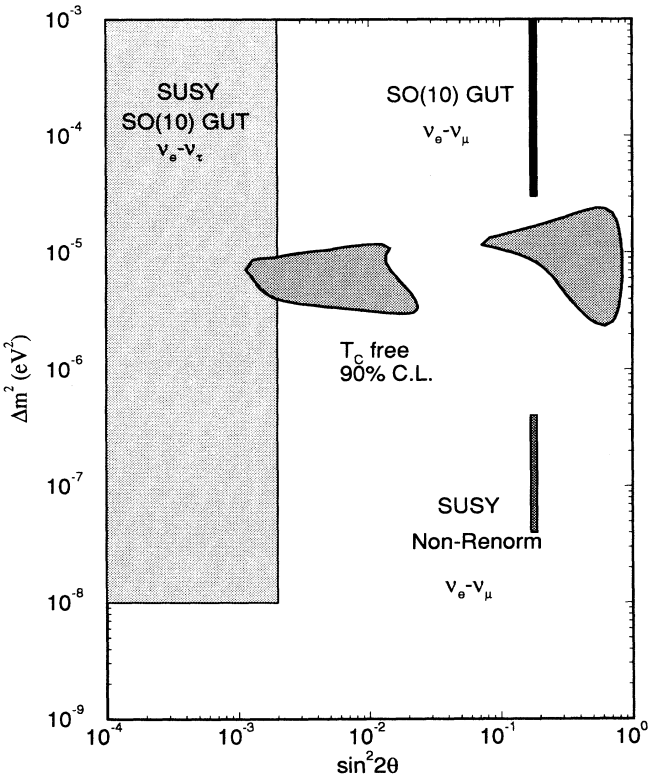

FIG. 12. The allowed MSW region of the combined result of Homestake, Kamiokande II+III, SAGE, and GALLEX, using T_c as a free parameter. As a result of allowing T_c to change, the 90% C.L. region is wider than in Fig. 6(a). Also shown are Δm^2, $\sin^2 2\theta$ predicted by SUSY SO(10) GUT's (shaded), intermediate-scale SO(10) GUT's (thick line), and string-inspired SUSY models with nonrenormalizable operators (shaded line). In each model the predictions for Δm^2 are not robust and easy to change. In the string-inspired model, $\sin^2 2\theta$ is also changeable.

ture Sun allows a region between the two islands allowed in the SSM case [Fig. 6(a)], while the cooler Sun pushes the parameter-space outward.

From the Bahcall-Ulrich paper [8] we have estimated the uncertainty of the central temperature as 0.57%. Turck-Chièse compares [28] the central temperatures of four SSM's [8,10,29,30]: they agree within 1.3%. The changes by 5% in Fig. 13(a) and 13(b) are very large compared to these uncertainties. (The best fit 13–14% reduction for the gallium results in the cooler Sun model is impossibly large unless the SSM is drastically modified.) We have also calculated the MSW fit with a more conservative uncertainty of T_c. Figure 14 shows the allowed region when $\Delta T_c = 0.02$. The fits when T_c is fixed at 1.03 and 0.98 are shown in Fig. 15 and Fig. 16; the allowed regions are still consistent with the grand unified theory (GUT) predictions.

V. THEORETICAL IMPLICATION OF FITTED MSW PARAMETERS

The best-fit MSW parameters from Fig. 6(a) and Fig. 11 are summarized in Table III for the SSM and for non-SSM in which T_c is an adjustable parameter. The results for sterile-neutrino oscillations are listed in Table IV. The Δm^2 range is consistent with the general expectations of grand unified theories [16] or string-inspired models [18], but the mixing angles are not in agreement with the expectation $\theta_{\text{lepton}} \sim \theta_{\text{CKM}}$ of the simplest GUT's [16]. If we accept the SSM, the observed neutrino mixing are at least four times larger (or considerably smaller) than the quark mixings, $\sin^2 2\theta = 0.18$ and $< 2 \times 10^{-3}$ for *u-c* and *u-t* quarks, respectively. If we allow a warm Sun, then Cabibbo mixing with $\Delta m^2 \simeq (0.8-2) \times 10^{-5}$ eV^2 is possible; this suggests $m_{\nu_\mu} \simeq (3-4) \times 10^{-3}$ eV and an SO(10) GUT with intermediate-scale symmetry breaking. If we allow a cool Sun, then $\Delta m^2 \simeq (0.5-1.5) \times 10^{-5}$ eV^2 is possible, suggesting $m_{\nu_\tau} \simeq (2-4) \times 10^{-3}$ eV and a supersymmetric (SUSY) SO(10) GUT (with large Higgs representations so that the seesaw scale is close to the unification scale).

GUT predictions for neutrino masses are much less robust than for mixing angles and mass ratios. We therefore regard the seesaw model [31] only as a crude guide to neutrino masses. In the SUSY GUT case, all neutrino masses are cosmologically and astrophysically insignificant. In the non-SUSY SO(10) GUT, the seesaw model suggests cosmologically interesting ν_τ masses. Since $m_t/m_c \sim 100$ and $m_\tau/m_\mu = 17$ we have $m_{\nu_\tau} \simeq 0.4-0.8$ (40–80) eV for a linear (quadratic) seesaw model with up-quark masses and $m_{\nu_\tau} \simeq 0.07-0.14$ (1–2) eV for a linear (quadratic) seesaw model with charged lepton masses. In carrying out these extrapolations, we have taken $m_{\nu_\mu} \simeq (2-4) \times 10^{-3}$ eV and, for the up-quark case, have included a factor 2 to renormalize mass ratio from GUT to low-energy scales [16]. (This factor increases beyond two nonlinearly for large value of the top-quark mass because of the Higgs corrections to the

top-quark mass [32].) We see that only an intermediate scale quadratic seesaw mechanism can give cosmologically significant ν_τ mass [16]. String-inspired models can generate an intermediate seesaw scale via effective nonrenormalizable operators [18]. There are no clear mixing angle predictions in such models, but for $\nu_e \rightarrow \nu_\mu$ oscillations consistent with either MSW solution, the ν_τ may again be cosmologically significant.

The smaller values of m_{ν_τ} would not be cosmologically relevant, but could affect the flux of atmospheric ν_μ if the ν_μ-ν_τ mixing angle is unexpectedly near maximal.

VI. PROSPECTS FOR FUTURE EXPERIMENTS

One can predict the results of future solar neutrino observations from the parameters of the combined fit [Fig. 6(a)]. The ν_e survival probability is shown as a function of energy in Fig. 17 for each of the allowed regions. The predicted observed rates for the high-energy ^{8}B ν_e-e scattering (SNO [33] and Super-Kamiokande [34]), the ν_e-d reaction (SNO), and the ν_e-e scattering from ^{7}Be neutrinos (BOREXINO [35]) are listed in Table V [36].

TABLE V. Predicted rates for future solar neutrino detectors, relative to the SSM expectations. The rates are listed for each of the allowed regions obtained from the best fit [Fig. 6 (a)].

	Rate/SSM	
	Nonadiabatic	Large mixing
SNO (charged current)	0.15–0.5	0.15–0.3
SNO (ν-e scattering)	0.3–0.6	0.3–0.45
Super-Kamiokande	0.3–0.6	0.3–0.45
Borexino (^{7}Be ν-e)	0.25–0.7	0.45–0.65

The detector cross sections as well as the proposed energy resolution of the detectors are included in the calculation.

The measurement of the charged current reaction $\nu_e + d \rightarrow e + p + p$, which is planned for the first-year operation of SNO would be a clear diagnostic of the MSW; the distortion of the energy spectrum is characteristic of most particle physics solutions of the solar neutrino problem and cannot be caused by any astrophysical effects operative in the Sun [37]. Figure 18 shows the predicted energy spectra for both the nonadiabatic and the large-mixing solution, along with estimated statistical

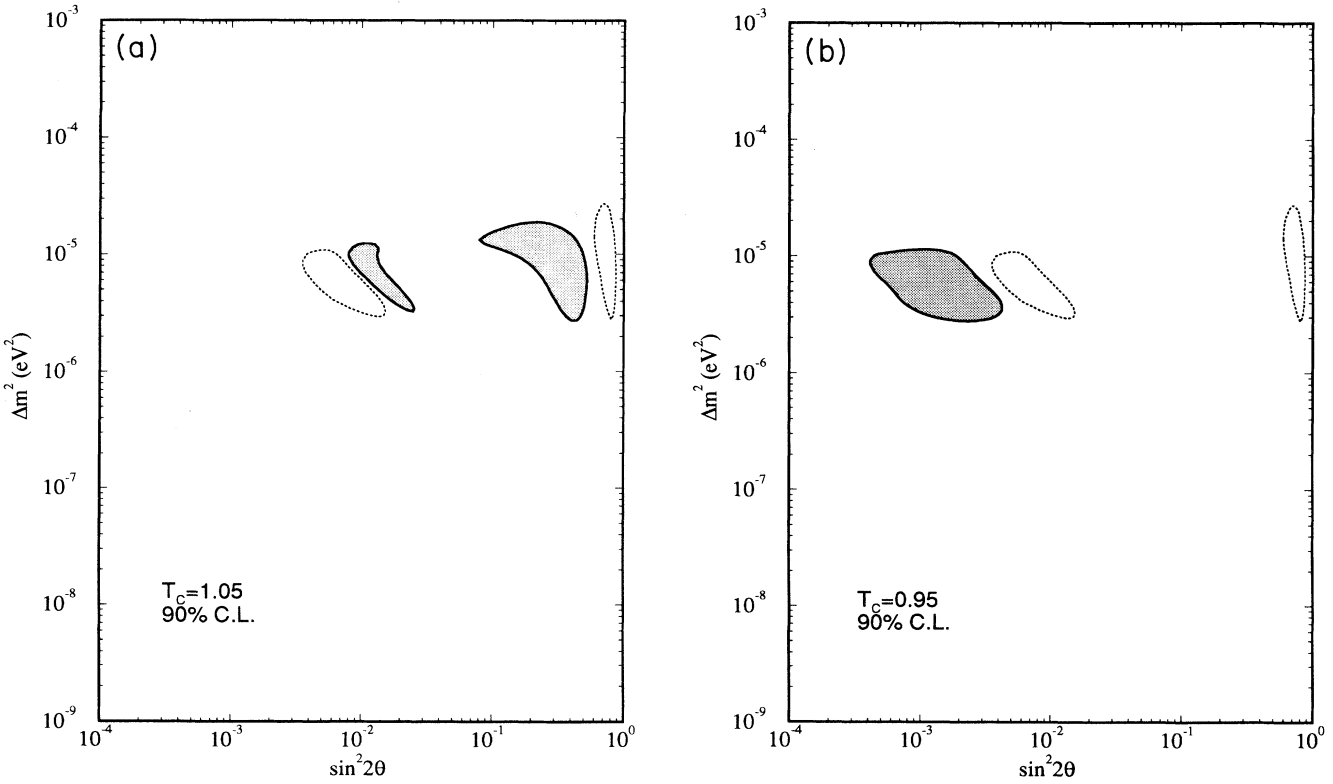

FIG. 13. (a) The shaded shows the allowed MSW region of the combined result of Homestake, Kamiokande II+III, SAGE, and GALLEX when T_c is fixed at 1.05 (a warmer Sun). The dotted regions are those allowed by the SSM [Fig. 6(a)]. As a result of the high T_c, the parameters predicted by SO(10) GUT's with intermediate-breaking scales are allowed. (b) The shading shows the allowed MSW region of the combined result of Homestake, Kamiokande II+III, SAGE, and GALLEX when T_c is fixed at 0.95 (a cooler Sun). The SSM allowed regions are again shown as dotted. As a result of the lowering T_c, the allowed region is now consistent with supersymmetric SO(10) GUT predictions.

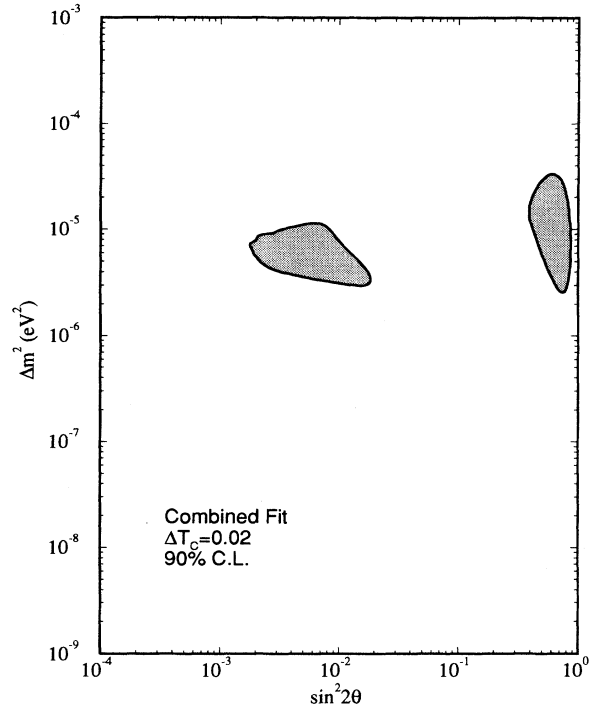

FIG. 14. The MSW parameters allowed by the combined data when the theoretical uncertainty in T_c is enlarged from 0.6% to 2% (shaded region).

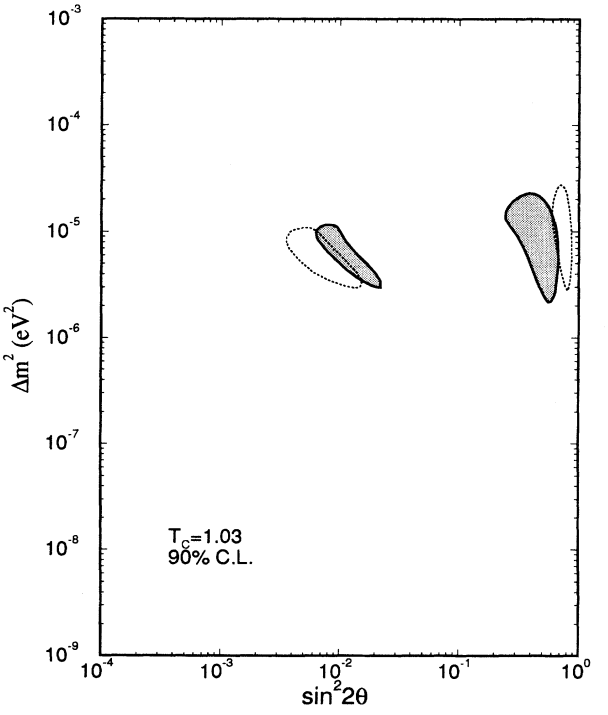

FIG. 15. The MSW parameters allowed by the combined data in the SSM (dotted lines) and in the 3% warmer solar model (shaded region). The large-angle solution allowed by a warmer Sun is consistent with the predictions of the intermediate-scale SO(10) GUT's.

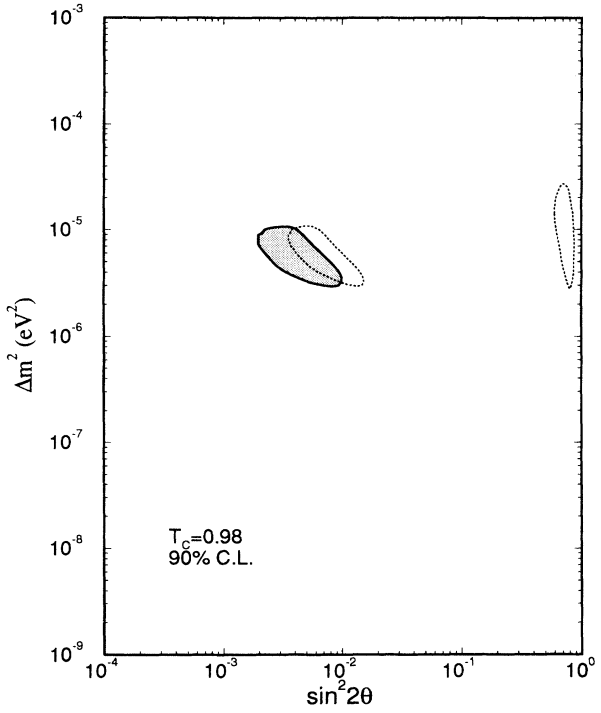

FIG. 16. The MSW parameters allowed by the combined data in the SSM (dotted lines) and in the 2% cooler solar model (shaded region). The nonadiabatic solution allowed by a cooler Sun is consistent with the predictions of the SUSY SO(10) GUT.

errors equivalent to a two-year operation (6000 total events). The nonadiabatic spectrum is very similar to the predicted spectrum for sterile neutrinos. If there is a nonadiabatic MSW effect, as suggested by the best fit (Table III), the spectral distortion would (a) confirm the MSW effect, and (b) discriminate between the two

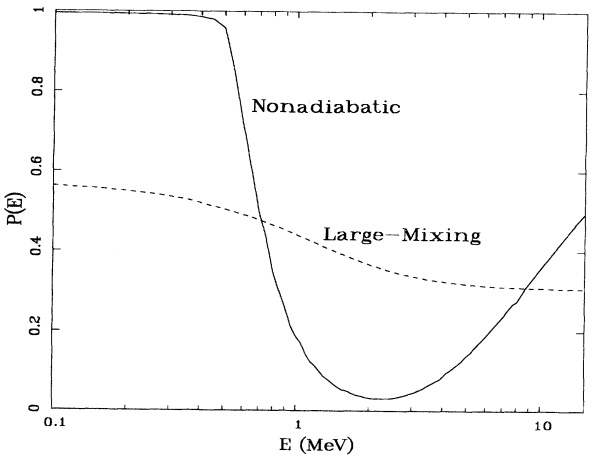

FIG. 17. The ν_e survival probabilities as a function of energy for the two regions obtained by SSM [Fig. 6(a)]. The solid line is for the nonadiabatic region and the dashed line is for the large-mixing region.

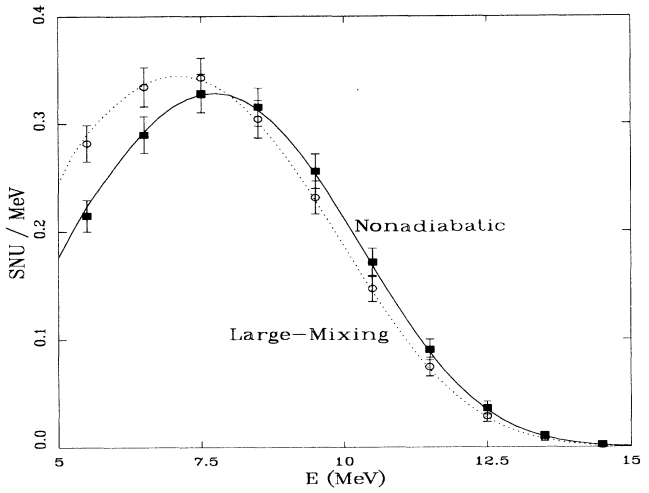

FIG. 18. The predicted spectral shape of charged-current events at SNO. The solid line is for the allowed parameter space in the nonadiabatic region, and the dashed line is for the large-mixing region. The errors are equivalent to a two-year operation (6000 events). The distortion of the spectrum in the nonadiabatic branch will confirm the MSW effect and differentiate the two allowed regions [Fig. 6(a)].

presently allowed solutions. Of course, the neutral to charged current ratio would also establish MSW oscillations into ν_μ or ν_τ (but not into a sterile ν).

The measurements of the neutral current events by SNO and BOREXINO, and their ratio relative to the charged current events would provide definite evidence for MSW flavor oscillations. The neutral current mode can determine the core temperature precisely even in the presence of the MSW effect: assuming 10% systematic errors, the high sensitivity of the ^{8}B neutrino flux ($\sim T_c^{18}$) allows a determination of T_c at the 0.5% level.

VII. SUMMARY

Existing Homestake, Kamiokande, and GALLEX experiments strongly disfavor astrophysical solutions invoking a cooler Sun. For the matter-enhanced neutrino oscillations, the data constrain the parameter space to two small regions, one in the nonadiabatic region (which is preferred by the data) and one in the large-mixing region. The fit for oscillations into a sterile neutrino allows only nonadiabatic oscillations at 90% C.L. Allowing a non-standard core temperature along with MSW oscillations we find that the data constrain the core temperature at the 5% level, yielding values consistent with the SSM. The warmer Sun ($T_c = 1.05$) allows the parameter space predicted by the SO(10) GUT with an intermediate-breaking scale (for which the ν_τ may be cosmologically relevant), while the cooler Sun stretches the allowed parameters into a region predicted by simple supersymmetric SO(10) GUT's. Superstring-inspired models are consistent with all solutions. Predictions are made for future solar neutrino detectors.

ACKNOWLEDGMENTS

We thank John Bahcall and Marc Pinsonneault for providing us with the solar model and neutrino fluxes in computer-readable form. We also thank Satoshi Nozawa for the ν-d cross-section subroutine. It is a pleasure to thank Eugene Beier and Marc Pinsonneault for useful discussions. One of us (N.H.) is indebted to Ed Frank for invaluable advice in computations. This work was supported by the Department of Energy Contract Nos. DE-AC02-76-ERO-3071 and DE-FG02-88ER40479.

[1] R. Davis, Jr. *et al.*, in *Proceedings of the 21st International Cosmic Ray Conference,* Adelaide, Australia, 1989, edited by R. J. Protheroe (University of Adelaide Press, Adelaide, 1990), Vol. 12, p. 143.

[2] J. N. Bahcall and M. H. Pinsonneault, Rev. Mod. Phys. **64**, 885 (1992).

[3] K. S. Hirata *et al.*, Phys. Rev. Lett. **65**, 1297 (1990); **65**, 1301 (1990); **66**, 9 (1991).

[4] Y. Suzuki, in International Symposium on Neutrino Astrophysics, Takayama, Kamioka, 1992 (unpublished). The reported rate (for Kamokande II and 395 days of Kamiokande III) is 0.49±0.04 (stat) ±0.06 (syst) relative to the Bahcall and Ulrich SSM. We use a value renormalized to the Bahcall and Pinsonneault SSM.

[5] GALLEX Collaboration, P. Anselmann *et al.*, Phys. Lett. B **285**, 376 (1992); **285**, 390 (1992).

[6] A. I. Abazov *et al.*, Phys. Rev. Lett. **67**, 3332 (1991).

[7] V. N. Gavlin, in *Proceedings of the XXVI International Conference on High Energy Physics,* Dallas, Texas, 1992, edited by J. Sanford (AIP, New York, 1993).

[8] J. N. Bahcall and R. N. Ulrich, Rev. Mod. Phys. **60**, 297 (1988); J. N. Bahcall, *Neutrino Astrophysics* (Cambridge University Press, Cambridge, England, 1989).

[9] R. Sienkiewicz, J. N. Bahcall, and B. Paczyński, Astrophys. J. **349**, 641 (1990).

[10] S. Turck-Chièze, S. Cahen, M. Cassé, and C. Doom, Astrophys. J. **335**, 415 (1988).

[11] S. Turck-Chièze, in XV International Conference on Neutrino Physics and Astrophysics, Granada, 1992 (unpublished).

[12] J. Christensen-Dalsgaard, D. O. Gough, and J. Toomre, Science **229**, 923 (1985).

[13] The following analysis is an updated version of that given by S. A. Bludman, D. C. Kennedy, and P. G. Langacker, Phys. Rev. D **45**, 1810 (1992); Nucl. Phys. **B373**, 498 (1992); a similar analysis is given in Ref. [5].

[14] J. Faulkner and R. L. Gilliland, Astrophys. J. **299**, 994 (1985); R. L. Gilliland, J. Faulkner, W. H. Press, and D. N. Spergel, *ibid.* **306**, 703 (1986).

[15] See Fig. 11 of Bahcall and Ulrich [8] or Fig. 6.2 and 6.3 of Bahcall [8].

[16] See Bludman, Kennedy, and Langacker [13].

[17] L. Wolfenstein, Phys. Rev. D **17**, 2369 (1978); **20**, 2634 (1979); S. P. Mikheyev and A. Yu. Smirnov, Yad. Fiz. **42**, 1441 (1985) [Sov. J. Nucl. Phys. **42**, 913 (1985)]; Nuovo Cimento **9C**, 17 (1986).

[18] M. Cvetič and P. G. Langacker, Phys. Rev. D **46**, R2759 (1992).

[19] S. J. Parke, Phys. Rev. Lett. **57**, 1275 (1986). For calculations of survival probabilities, see also W. C. Haxton, Phys. Rev. D **35**, 2352 (1987); D. C. Kennedy, University of Pennsylvania Report No. UPR 0442-T (REV), 1992 (unpublished); S. T. Petcov [20].

[20] P. Pizzochero, Phys. Rev. D **36**, 2293 (1987); S. T. Petcov, Phys. Lett. B **200**, 373 (1988); in *Weak Interactions and Neutrinos,* Proceedings of the Twelfth International Workshop, Ginosar, Israel, 1989, edited by P. Singer and B. Gad Eilam [Nucl. Phys. B (Proc. Suppl.) **13**, 527 (1990)].

[21] L. D. Landau, Phys. Z. Sowjetunion **1**, 88 (1932); **2**, 46 (1932); C. Zener, Proc. R. Soc. London **137**, 696 (1932).

[22] K. S. Hirata *et al.*, Phys. Rev. D **44**, 2241 (1991).

[23] J. N. Bahcall and W. C. Haxton, Phys. Rev. D **40**, 931 (1989).

[24] X. Shi, D. N. Schramm, and J. N. Bahcall, Phys. Rev. Lett. **69**, 717 (1992).

[25] P.G. Langacker, University of Pennsylvania Report No. UPR 0401T, 1989 (unpublished); R. Barbieri and A. Dolgov, Nucl. Phys. **B349**, 743 (1991); K. Enqvist, K. Kainulainen, and J. Maalampi, Phys. Lett. B **249**, 531 (1990); M. J. Thomson and B. H. J. McKellar, *ibid.* **259**, 113 (1991); V. Barger *et al.*, Phys. Rev. D **43**, 1759 (1991); P. Langacker and J. Liu, *ibid.* **46**, 4140 (1992).

[26] D. O. Caldwell and P. G. Langacker, Phys. Rev. D **44**, 823 (1991).

[27] A similar constraint on T_c is obtained by a different approach by H. A. Bethe and J. N. Bahcall, Phys. Rev. D **44**, 2962 (1991).

[28] S. Turck-Chièze, Service d'Astrophysique Report No. 1992/32, 1992 (unpublished).

[29] A. N. Cox, J. A. Guzik, and R. B. Kidman, Astrophys. J. **335**, 415 (1988).

[30] I. J. Sackmann, A. I. Boothroyd, and W. A. Fowler, Astrophys. J **360**, 727 (1990).

[31] M. Gell-Mann, P. Ramond, and R. Slansky, in *Supergravity,* Proceedings of the Workshop, Stony Brook, New York, 1989, edited by P. van Nieuwenhuizen and D. Freedman (North-Holland, Amsterdam, 1979), p. 315; T. Yanagida, Prog. Theor. Phys. **B135**, 66 (1978).

[32] D. C. Kennedy, Phys. Lett. B (to be published).

[33] G. T. Ewan *et al.*, "Sudbury Neutrino Observatory Proposal," Report No. SNO-87-12, 1987 (unpublished); "Scientific and Technical Description of the Mark II SNO Detector," edited by E. W. Beier and D. Sinclair, Report No. SNO-89-15, 1989 (unpublished).

[34] Y. Totsuka, University of Tokyo (ICRR) Report No. ICCR-Report 227-90-20, 1990 (unpublished).

[35] Borexino at Gran Sasso—Proposal for a Real Time Detector for Low Energy Solar Neutrinos, edited by G. Bellini, M. Campanella, D. Giugni, and R. Raghavan (unpublished), Vol. 1.

[36] Similar predictions for BOREXINO are discussed by J. M. Gelb, W. Kwong, and S. P. Rosen, Phys. Rev. Lett. **69**, 1846 (1992); W. Kwong and S. P. Rosen, *ibid.* **68**, 748 (1992). See also P. I. Krastev and S. T. Petcov, CERN Report No. CERN-TH.6539/92 (unpublished).

[37] J. N. Bahcall, Phys. Rev. D **44**, 1644 (1991).